Article

Enhanced Adsorption of Azoxystrobin from Water by As-Prepared Silica Nanoparticles

Farag Malhat [1], Osama I. Abdallah [1,*], Mohamed Hussien [2,3], Ahmed M. Youssef [4], Fahad M. Alminderej [5,*] and Sayed M. Saleh [5,6]

[1] Department of Pesticide Residues Analysis and Environmental Pollution, Central Agricultural Pesticide Laboratory (CAPL), Agricultural Research Center (ARC), Dokki, Giza 12618, Egypt; fmmalhat@capl.gov.eg

[2] Department of Chemistry, Faculty of Science, King Khalid University, Abha 61413, Saudi Arabia; mhalmosylhy@kku.edu.sa

[3] Department of Pesticide Formulation, Central Agricultural Pesticide Laboratory (CAPL), Agricultural Research Center (ARC), Dokki, Giza 12618, Egypt

[4] Packaging Materials Department, National Research Centre, 33 El Bohouth St. (former El Tahrir St.), Dokki, Giza 12622, Egypt; ahmed.youssef@lgp2.grenoble-inp.fr

[5] Department of Chemistry, College of Science, Qassim University, Buraidah 52571, Saudi Arabia; e.saleh@qu.edu.sa

[6] Chemistry Branch, Department of Science and Mathematics, Faculty of Petroleum and Mining Engineering, Suez University, Suez 43721, Egypt

* Correspondence: oiabdullah@qassim.gov.sa (O.I.A.); f.alminderej@qu.edu.sa (F.M.A.); Tel.:+966-506174372 (O.I.A.); +996-6504488486 (F.M.A.)

Abstract: Nanoparticles are of great interest for water treatment as they remove a significant portion of water contaminants. In analogy to these emerging practices, the present work investigated the feasibility of using silica nanoparticles (SiO_2-NPs) to remove azoxystrobin from an aqueous solution. We investigated the effects of experimental parameters, such as solution temperature, adsorbent dosage, contact time, and initial azoxystrobin concentration, on the removal efficiency of azoxystrobin. Structural and chemical analysis of the synthesized nanoparticles was performing using X-ray diffraction patterns (XRD), scanning electron microscopy (SEM), dynamic light scattering (DLS), and surface studies. The percentage of azoxystrobin removal efficiency was 92.8 at an initial azoxystrobin concentration of 10 mg/L. The result showed that by increasing the adsorbent dosage from 0.005 to 0.1 mg, the percentage removal efficiency of azoxystrobin from aqueous solution increased significantly from 59.72% to 95.21%. At the same time, the adsorption amount of azoxystrobin in equilibrium decreased with increasing temperature. It was found that the optimum temperature for removing azoxystrobin was 20 °C. Although the study was conducted under well-controlled laboratory conditions, the silica nanoparticle system showed excellent performance in removing a significant amount of azoxystrobin, making it a potential alternative/cooperator in water treatment for removing pesticides from aqueous solutions.

Keywords: nanoparticles; azoxystrobin; adsorption; pesticides; water treatment

1. Introduction

Silicon dioxide (SiO_2) has been the subject of numerous studies due to its remarkable physical and chemical properties. Crystalline forms of SiO_2 include quartz, cristobalite, tridymite, stishovite, and coesite, with amorphous silica being the most common. Amorphous silica has been the subject of numerous fundamental studies, with investigations into its electrical structure, bond characterization, defects, and optical properties. Silicate compounds, of which silica is the most common, account for more than 95% of the Earth's rock surface [1]. They occurs in both crystalline and amorphous states. The Earth's crust is more crystalline, but it is difficult to use directly due to its low reactivity [2].

However, for the production of inorganic materials, a pure form of silica with few impurities and amorphous character is required [3]. Therefore, amorphous silica is used in a variety of manufacturing applications [2–10]; these include abrasives, refined materials (SiC, Si3N4), cement, ceramic pigments, glasses, refractory materials, microelectronics, mortars, and zeolites. Silica nanoparticles have stood out among the various types of manufactured nanoparticles [11–29] because they can be used in many fields of research and industry. Absorbents, thermal insulants, catalysts, and additives for cosmetics, pharmaceuticals, printer toners, paints, foods, and insecticides are just a few examples of the uses of these materials in these other fields [2,8]. The controlled release of drugs and biosensors [4–6,8,10] are two examples of nano-silica uses in biomedicine and biotechnology, especially in cancer treatment and DNA transfection. Therefore, they are mass-produced [23–25].

Various techniques can be used to synthesize silicon dioxide (SiO_2). There is a tremendous interest in synthesizing crystalline and uniform materials for applications in microelectronics, optics, electrical engineering, and other fields. The sol–gel process is a very flexible route for using wet chemical techniques to prepare various photonic materials in different configurations, such as monoliths, coatings, fibers, and films for optical applications [30]. The metal salt undergoes hydrolysis and polycondensation reactions to form a gel-like colloidal suspension consisting of a liquid solvent and a solid metal oxide phase, with morphologies ranging from discrete particles to continuous polymer networks [31].

Many processes have been used to treat wastewater contaminants, such as solvent extraction, chemical precipitation, membrane technologies, adsorption, membrane separation, and ion exchange [31]. Nanomaterials, such as silica nanoparticles, are considered novel methods for treating wastewater contaminants [32,33]. Silica obtained from the black liquor of rice husks has excellent properties and can be used as an adsorbent, especially for treating wastewater contaminated with dyes. The sol–gel process produces silica with precise particle size and distribution control, even at low temperatures. A solution of water and HCl was used as the silica source to prepare nanoscale particles [34] with a very high specific surface area and low density.

Pesticides are widely used in agriculture today to control pests and thereby increase production, but the excessive or improper use of pesticides can lead to many adverse effects, primarily environmental and water pollution [35]. In addition, the use of washing equipment to prepare and apply pesticides, and traces of pesticides in grey water after washing pesticide-contaminated products, contributes to the accumulation of pesticides in wastewater [36].

Wastewater from industries that produce chemicals and pesticides is also referred to as pesticide production wastewater and is added to domestic wastewater. Before being combined with domestic wastewater, pesticide production wastewater must undergo extensive treatment. Due to the high concentrations and resistance of pesticides in wastewater, the treatment of pesticides from water sources is an essential subject of study [37]. The acute and chronic toxicity of azoxystrobin (Figure 1) is low in humans, birds, mammals, and bees, but high in freshwater fish, freshwater invertebrates, estuarine/marine fish, and estuarine/marine invertebrates. In addition, among ecologically active pesticides, broad-spectrum fungicide azoxystrobin is considered hazardous to estuarine and freshwater fish [38]. Several studies have been conducted on solid sorbents to remove azoxystrobin via adsorption processes [39,40].
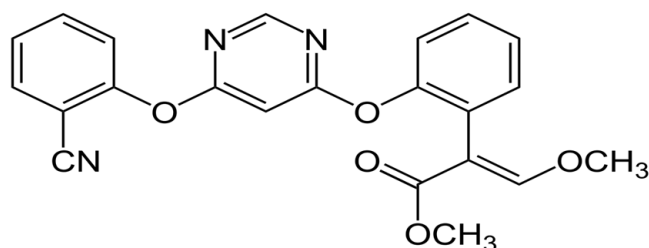
Figure 1. Chemical structure of azoxystrobin.

The present study aims to synthesize silica nanoparticles from tetraethoxysilane by a nontoxic, rapid, and one-step synthetic method that can be used to remove azoxystrobin residues from water. Using the composite as an adsorbent to remove azoxystrobin from aqueous solutions was investigated experimentally, and the results were discussed.

2. Materials and Methods

2.1. Materials

All reagents were of sufficient purity for use in analytical work. Tetraethoxysilone (TEOS) was purchased as a precursor from Sigma Aldrich (St. Louis, MO, USA) with a purity of 99.9% and was used for synthesis. Solvents such as ethanol and deionized water from Merck Chemical (Merck Ltd., Darmstadt, Germany) (purity 99.9%) rounded out the list of reagents.

2.2. Synthesis of Silica Nanoparticles

To prepare silica nanoparticles (SiO_2-NPs), we used the alkoxide route of the sol–gel technique. Tetraethoxysilane (TEOS) (1 mol) was dissolved in 10 mL ethanol, and the mixture was stirred with deionized water (35 mL) for 10 min. Then, 1 mol of catalyst HCl was dropped into the mix, and the mixture was magnetically swirled for another 50 min. When heated to 60 °C, the solution became uniformly white and clear. A gel was prepared from the prepared material and allowed to stand at room temperature for about 2 h. White SiO_2 powder was prepared by drying the obtained solutions at 110 degrees Celsius for six hours. The result was crystalline SiO_2 particles. To better understand the composition of the obtained powder, we calcined it at 300 °C for one hour. For clarity, the term "sample" refers to both dry (at 110 °C) and calcined (at 300 °C) SiO_2 powder samples designated for further characterization [39].

2.3. Characterization

The crystal structure of the filler powders was determined using a Philips X-ray diffractometer (PW 1930 generator, PW 1820 goniometer) (Woburn, MA, USA) with Cu.Kα radiation (45 kV, 40 mA, with $\lambda = 0.15418$ nm). Analysis scans were performed in the 2θ range from 5 to 80°, with a step size of 0.02 and a step time of 1 s. A Philips X-ray diffractometer (PW 1930 generator, PW 1820 goniometer) and Cu Kα radiation (45 kV, 40 mA, with $\lambda = 0.15418$ nm) were used to determine the crystal structure of the filler powders. The analysis scans covered a 2θ range of 5–80°, with a step size of 0.02° and step duration of 1 s. Scanning electron microscopy (SEM) (High-Resolution Quanta FEG 250-SEM) (Královopolská, Czech Republic) was used to study the nanomorphology of the synthesized SiO_2-NPs. The surfaces of the samples were analyzed in a low-level vacuum and without gold coating. Using the 632 nm line of a He–Ne laser as incident light at a 90° angle and a zeta potential with an exterior angle of 18.9°, a NICOMP 380 ZLS, dynamic light scattering (DLS) instrument (PSS, Santa Barbara, CA, USA) was used.

The Brunauer–Emmett–Teller (BET) theory was used to analyze the surface by placing St 2 on a NOVA touch 4LX from Quantachrome Instruments. Heating to high temperatures (110 °C) (Quantachrome Corporation, Boynton Beach, FL, USA) evaporated the water in the SiO_2 nanoparticles. After the SiO_2 nanoparticles were gassed with a constant stream of N_2 at 200 °C for 2 h, they were tested at room temperature. The desorption scientists used the Barrett–Joyner–Halenda (BJH) method to analyze the pore size distribution.

2.4. Utilization of Nano-Particles in the Removal of Azoxystrobin

Batch adsorption experiments were conducted whereby silica nanoparticles were immersed in wastewater containing azoxystrobin to investigate the effects of temperature, contact time, adsorbent dosage, and initial concentration of azoxystrobin on the efficiency of azoxystrobin removal from wastewater. Stock solution with a concentration of 1.0 g/L was prepared by dissolving azoxystrobin in ultrapure water. It had a resistivity of 18.2 MΩ·cm, a TOC < 10 ppb, and a bacterial count < 10 CFU/mL. The stock solution was used to

prepare a series of working solutions with different concentrations in ultrapure water. Subsequently, 5.0 mg of silica nanoparticles were diluted in 26 mL of deionized water in 50 mL centrifuge tubes, and initial concentrations of 10 mg/L were achieved by adding specific amounts of the azoxystrobin stock solutions. The tubes containing the solutions were shaken in a mechanical shaker at 300 rpm and 25 °C, and their contents were made up of 30 mL of deionized water. The adsorbed mixtures were centrifuged at 3000 rpm for 3 min to separate the supernatant. The concentration of residual azoxystrobin in the supernatant was determined using HPLC-DAD (Agilent Technologies Inc., Waldbronn, Germany). A standard calibration curve calculated the pesticide concentration after adsorption onto silica nanoparticles. The amount of pesticide adsorbed was calculated using the following equation:

$$q_e = (C_0 - C_t) \times V/m \times M \tag{1}$$

The adsorption capacity of a pesticide at time t is denoted by q_e, where C_0 is the initial concentration of the pesticide in milligrams per liter, C_t is the final concentration of the pesticide in milligrams per liter, V is the total volume of the suspension in liters, m is the mass of adsorbed material in grams, and M is the molecular weight of azoxystrobin (403.4 g/mol). The following formula was used to determine the percentage of age-related reduction in pesticide use.

$$\text{Adsorption } (\%) = [1 - C_t/C_0] \times 100 \tag{2}$$

C_t and C_0 are the concentration at time t and the initial concentration, respectively.

2.4.1. Effect of Contact Time

Portions of 0.05 g of silica nanoparticles were weighed and placed in a series of 50 mL centrifuge tubes containing 30 mL of 10 μg/mL azoxystrobin in deionized water. Then, the tubes were capped and shaken at 300 rpm. The mixtures were centrifuged at 3000 rpm for 3 min, the supernatant was collected, and approximately 2 mL of the solution was removed and filtered through a 0.22 μm nylon syringe filter at various times (3 min to 16 h).

2.4.2. Effect of Initial Concentration of Azoxystrobin

We weighted out 50 mg portions of silica nanoparticles and placed them in a series of 50 mL centrifuge tubes containing 30 mL of various concentrations of azoxystrobin in deionized water (5 μg/mL, 10 μg/mL, 20 μg/mL, and 40 μg/mL). The tubes were capped and shaken at 300 rpm for 0.5 h and 1 h. The mixtures were centrifuged at 3000 rpm for 3 min, the supernatant was collected, and approximately 2 mL of the solution was removed and filtered through a 0.22 μm nylon syringe filter.

2.4.3. Effect of Adsorbent Mass

A series of solutions were prepared with constant concentrations of 10 μg/mL azoxystrobin in 30 mL deionized water and placed in 50 mL screw-capped centrifuge tubes. Then, various amounts (0.005–0.1 g) of silica nanoparticles were added. The tubes were capped and shaken at 300 rpm for 1 h and left overnight to equilibrate. The mixtures were centrifuged at 3000 rpm for 3 min, the supernatant was collected, and approximately 2 mL of the solution was removed and filtered through a 0.22 μm nylon syringe filter.

2.4.4. Effect of Temperature

The adsorption behavior of azoxystrobin at the same initial concentration and equilibration time was studied as a function of temperature. 50 mg of various silica nanoparticles were dispersed in 30 mL solutions containing 10 mg/L azoxystrobin. The initial temperatures were set between 20 and 40 °C. The suspensions were then shaken with a mechanical shaker for two hours at room temperature.

2.5. Regeneration and Reusability

The regeneration and reusability of silica nanoparticles for azoxystrobin removal were investigated using adsorption and desorption experiments. A series of solutions (10 mL) with the same concentration of 5 μg ml^{-1} were prepared in deionized water, then 0.05 g of silica nanoparticles was added to a centrifuge tube. This was then shaken at 300 rpm for 1 h. About 2 mL of the solution was withdrawn, filtered through a 0.22 μm syringe nylon filter, transferred to autosampler vials, and analyzed by HPLC as before. Then, the loaded silica nanoparticles from this first run were filtered and carefully washed several times with deionized water. The resulting solid was cured at 80 °C for 24 h before calcination at 100 to 600 °C for 10 h. Before the particles were used for the adsorption tests, they were degassed for 12 h. Then, another prepared solution of 10 mL/L azoxystrobin was added, and the second run was performed in the same order; the third, fourth, and fifth runs were performed similarly.

2.6. HPLC-DAD

The residual concentration of azoxystrobin was determined using a high-performance liquid chromatograph (HPLC), Agilent 1260 (Agilent Technologies Inc., Waldbronn, Germany), equipped with an autoinjector and a photodiode array detector (DAD) and a Zorbax XDB C-18 column (25 mm × 4.6 mm × 5 μm) (Agilent Technologies Inc., Waldbronn, Germany). The absorption wavelength was 230 nm. The mobile phase was acetonitrile: water (60:40, *v*/*v*), and the flow rate was 1 mL/min.

3. Results

3.1. Particle Size

Dynamic light scattering was used to determine the particle size of the prepared SiO$_2$ nanoparticles. Figure 2 shows the Gaussian distributions for SiO$_2$-NPs via intensity, volume, and number of weights. The average particle size and polydispersity variation index are shown in (Figure 2). The polydispersity of the generated SiO$_2$-NPs implies a narrow range of particle sizes, which is consistent with the comparable literature data for other nanoparticles, and the average diameter of the SiO$_2$-NPs was about 318 nm. The mean diameters of the individual nanomaterials vary considerably (Figure 2), although the particle distribution is excellent, and the mean particle diameters are homogeneous.
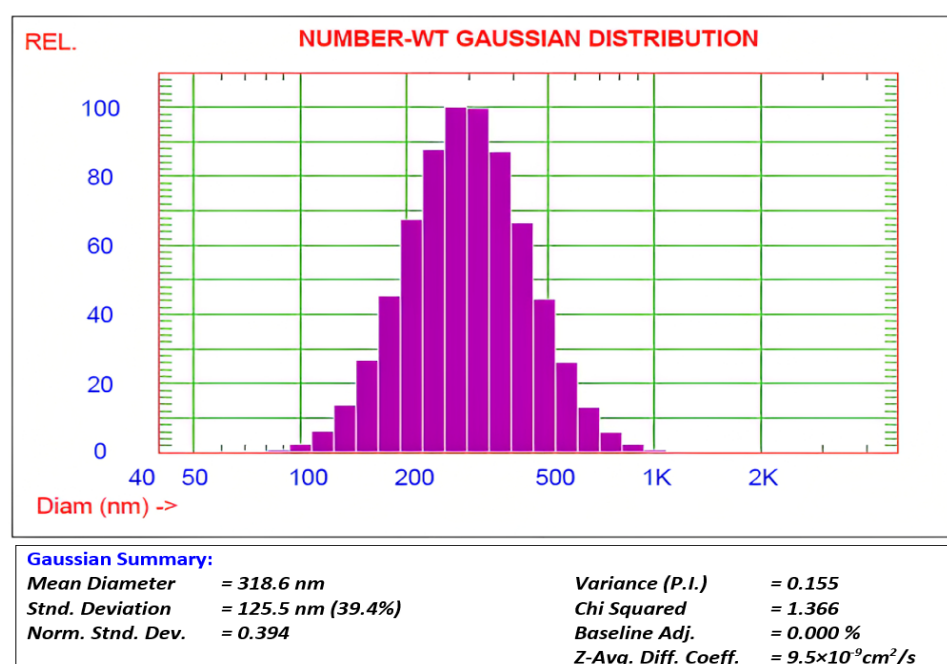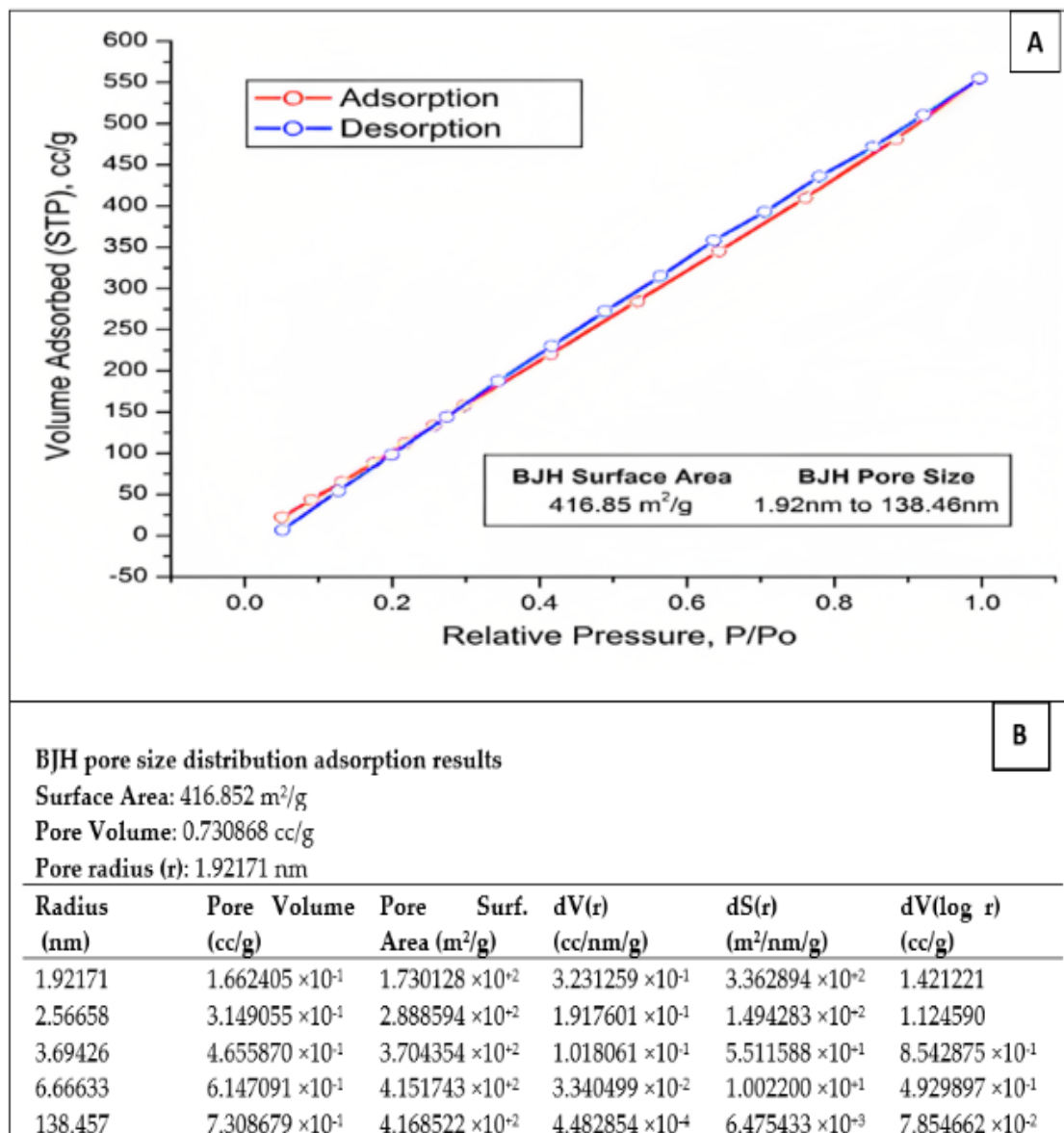

Figure 2. Dynamic light scattering distribution of SiO$_2$ nanoparticles.

3.2. Surface Area Evaluation

The specific surface area of the prepared SiO_2 nanoparticles was determined using the BET technique. In addition, the adsorption–desorption isotherms of SiO_2 nanoparticles and the pore size distribution were determined using nitrogen adsorption–desorption isotherms (Figure 3A). The nitrogen adsorption–desorption isotherms of SiO_2-NPs showed an H3 hysteresis loop at a relative pressure (P/Po) close to one. This could be classified as IV according to the IUPAC classification. This indicates the presence of a large number of meso- and macropores within the whole SiO_2-NP matrix. Moreover, the BJH analysis of the SiO_2-NPs shows a specific surface area of 416.85 m^2/g for the fabricated SiO_2-NPs. The obtained data confirm the results of the absorption measurements. The pore sizes of the SiO_2-NPs range from 1.92 to 138.46 nm, indicating the presence of mesopores (Figure 3B).


BJH pore size distribution adsorption results
Surface Area: 416.852 m^2/g
Pore Volume: 0.730868 cc/g
Pore radius (r): 1.92171 nm

Radius (nm)	Pore Volume (cc/g)	Pore Surf. Area (m^2/g)	dV(r) (cc/nm/g)	dS(r) $(m^2/nm/g)$	dV(log r) (cc/g)
1.92171	1.662405×10^{-1}	$1.730128 \times 10^{+2}$	3.231259×10^{-1}	$3.362894 \times 10^{+2}$	1.421221
2.56658	3.149055×10^{-1}	$2.888594 \times 10^{+2}$	1.917601×10^{-1}	1.494283×10^{-2}	1.124590
3.69426	4.655870×10^{-1}	$3.704354 \times 10^{+2}$	1.018061×10^{-1}	$5.511588 \times 10^{+1}$	8.542875×10^{-1}
6.66633	6.147091×10^{-1}	$4.151743 \times 10^{+2}$	3.340499×10^{-2}	$1.002200 \times 10^{+1}$	4.929897×10^{-1}
138.457	7.308679×10^{-1}	$4.168522 \times 10^{+2}$	4.482854×10^{-4}	6.475433×10^{-3}	7.854662×10^{-2}

Figure 3. (**A**) BET adsorption–desorption surface area analysis of the prepared SiO_2-NPs. (**B**) The pore size distribution adsorption results of SiO_2-NPs.

3.3. Surface Characterization

A scanning electron microscope (SEM) was used to study the morphology of the fabricated SiO_2-NPs. Among the critical factors controlling the fabrication conditions are

the solvent, water content, concentration, and type of catalyst used. It was found that factors affecting the overall stability of the sol are a significant amount of hydrochloric acid and TEOS, as well as the sol preparation steps mentioned above. As for the stability of the sol in the quench reaction, the change in HCl resulted in immediate precipitation and inhomogeneity. The pretreatment of TEOS with hydrochloric acid resulted in a strong initial exothermic reaction and rapid gelation. Figure 4 shows the SEM micrographs of SiO_2-NPs dried at 110 °C and prepared at a calcination temperature. The synthesized particles have well-defined spherical particles, as shown in Figure 4A,B. Accordingly, it can be seen that SiO_2-NPs calcined at 300 °C have a spherical morphology and regular shape.
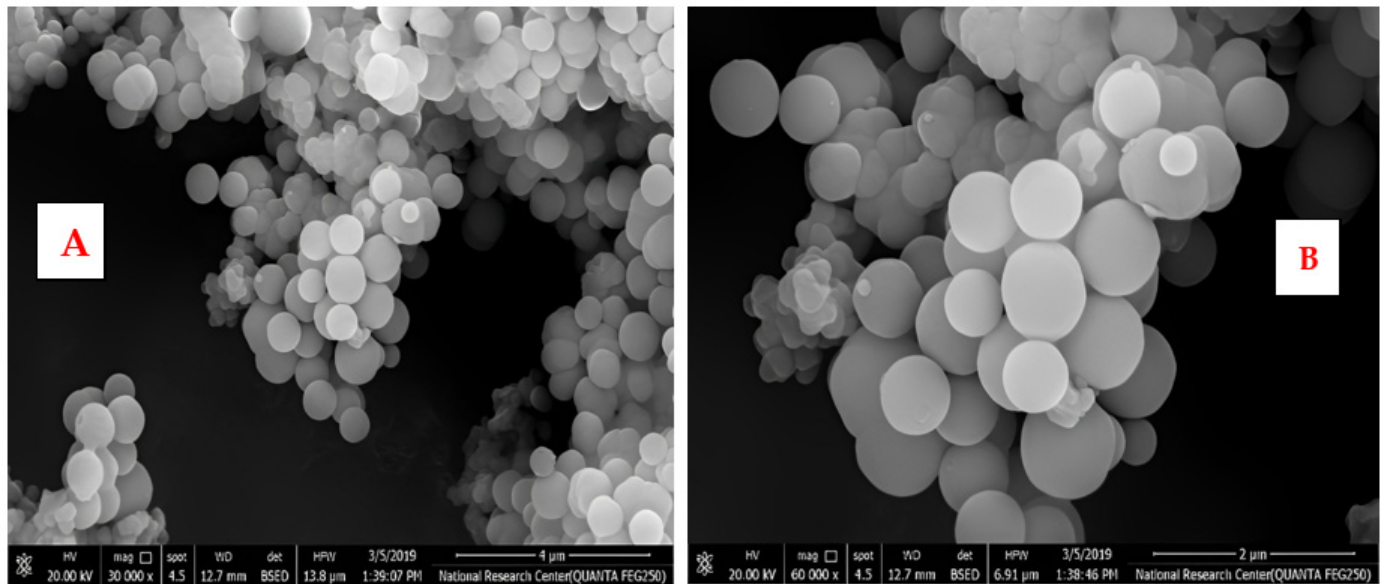
Figure 4. (**A**,**B**): SEM images of SiO_2 nanoparticles with different magnifications.
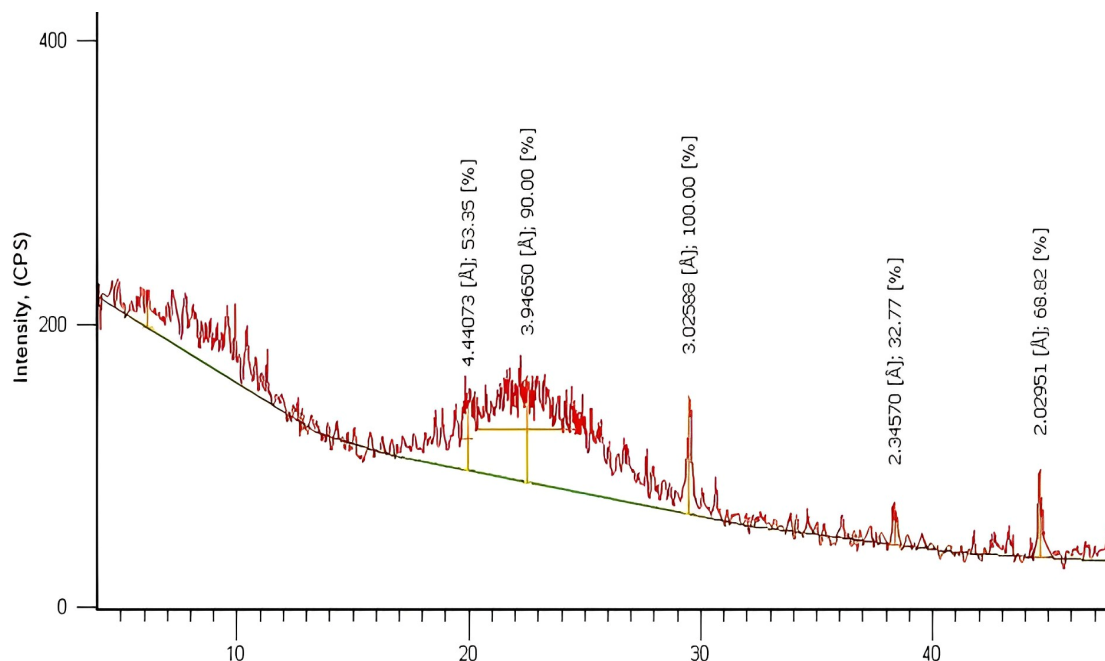
3.4. XRD Analysis of SiO₂ Nanoparticles

X-ray diffraction (XRD) patterns were studied on SiO_2-NPs in powder form, and the characteristic diffraction patterns are shown in Figure 5. From this figure, the size of the sub-micrometer particles or crystallites can be determined using the Debye–Scherer equation as follows:

$$D = K \lambda / \beta \cos\theta$$

where D is the average crystallite size, K is a constant for crystallite shape (0.9), X-ray wavelength (in this case Å for Cu-Kα radiation), β is the full width at half maxima (FWHM), and θ is the Bragg angle. This equation can be used to describe the size of the SiO_2-NPs produced.

The data obtained from the XRD spectrum were compared with the data from JCPDS Card #850335 for SiO_2 [41]. It can be promised that the material formed is SiO_2 NPs since the peaks indicate the formation of particles with dimensions in the nanometer range and back reflection at planes (100), (110), (102), (111), (200), and (201) at 2θ values 20. 14°, 22.21°, 29.49°, 38.97°, 41.75°, and 44.90°, respectively, for the sample prepared via the sol–gel technique. From the XRD pattern, it can be determined that the fabricated nanomaterial has a hexagonal crystal structure and an original lattice with lattice parameters of a = b = 4.913 Å and c = 5.405 Å. The XRD peaks were sharper when the SiO_2 NPs were calcined at 300 °C, and the crystallite size was about 55 nm. Therefore, it can be concluded that increasing the heat treatment to 300 °C causes the uniform crystallization of the SiO_2-NPs material.

Figure 5. XRD analysis of SiO$_2$ nanoparticles.

3.5. Adsorption Studies

3.5.1. Adsorbent Dose Influence

The dosage of adsorbent is crucial as it establishes the balance between adsorbent and adsorbate in the system and determines the capacity of the adsorbent to address given concentration of azoxystrobin. The effect of nano-silica dosing determines the capacity of these adsorbents to address a given azoxystrobin concentration and the balance between adsorbent and adsorbate in the system. The removal efficiency of azoxystrobin by nano-silica as a function of adsorbent dosage is shown in Figure 5, where all other experimental parameters were held constant at an azoxystrobin concentration of 10 mg/L, a shaking speed of 100 rpm, and a contact time of 24 h. The dosage of the nano-silica adsorbent varied from 0.005 to 0.1 g (Table 1).

Table 1. Effect of adsorbent dosage on removal efficiency %.

Mass of Adsorbent (g)	Initial Concentration of Azoxystrobin C$_o$ (mg/L)	Residual Concentration C$_e$ (mg/L)	q$_e$ (μmol/g^{-1})	Removal (%)
0.005	10	4.03	4818.9	59.7 ± 2.1
0.01	10	2.01	3223.3	79.9 ± 1.7
0.05	10	0.49	767.3	95.1 ± 2.7
0.1	10	0.47	719.2	95.6 ± 3.1

In this study, the percent removal efficiency of azoxystrobin at a concentration of 10 mg/L from an aqueous solution was significantly increased from 59.7% to 95.1% by increasing the adsorbent dosage. This observation can be explained by the increase in available active sites on the nano-silica surfaces, leading to an increasing number of binding sites for azoxystrobin.

3.5.2. Influence of Azoxystrobin Initial Concentration

Initial concentration is essential in overcoming the mass transfer barrier of azoxystrobin between the aqueous and solid phases. At an initial azoxystrobin concentration of 5 mg/L and a contact time of 0.5 and 1 h, the percent efficacy of azoxystrobin removal was 80.5 and 92.8, respectively (Table 2). Increasing the initial azoxystrobin concentration in an

aqueous solution decreased the removal efficiency of azoxystrobin. This observation could be attributed to the saturation of the availability of active adsorption sites on the nano-silica surface at higher azoxystrobin concentration, leading to an increase in the amount of azoxystrobin in the aqueous solution and, thus, a decrease in the percent removal efficiency of azoxystrobin. This effect can also be explained by the observation that more energetic sites are used for sorbate sorption at a low ratio of sorbate to sorbent. However, at higher concentrations of azoxystrobin solution, the more energetic sites are saturated, and the less energetic sites are used for sorption, resulting in a decrease in percentage removal.

Table 2. Influence of azoxystrobin initial concentration on removal efficiency.

Initial Concentration C_0 (mg/L)	Time (h)	Mass of Adsorbent (g)	Residual Concentration C_e (mg/L)	q_e (μmol/g)	Removal (%)
5	0.5	0.05	0.98	324.6	80.5 ± 2.4
5	1	0.05	0.36	374.5	92.8 ± 2.8
10	0.5	0.05	3.33	538.1	66.7 ± 1.3
10	1	0.05	2.52	603.9	74.9 ± 1.9
20	0.5	0.05	9.04	1045.1	54.8 ± 2.3
20	1	0.05	6.82	901.3	65.9 ± 3.7
40	0.5	0.05	20.24	1593.7	49.4 ± 3.1
40	1	0.05	18.64	2529.7	53.4 ± 4.1
80	0.5	0.05	44.6	2250.8	44.25 ± 3.3
80	1	0.05	39.12	25,531.2	51.1 ± 3.9

3.5.3. The Influence of Temperature

The effect of temperature on the adsorption of azoxystrobin on SiO$_2$-NPs was studied in the range of 20 °C to 40 °C, while the other factors were fixed. The residual concentration was measured, and the adsorbed amount and removal percentage were calculated using Equations (1) and (2), respectively. The removal efficiency in % varied with the temperature of the solution, as shown in Figure 6. The adsorption amount of azoxystrobin at equilibrium decreased at 40 °C due to the desorption of the azoxystrobin molecules that tended to migrate from the solid phase to the main phase when the solution was heated [41].
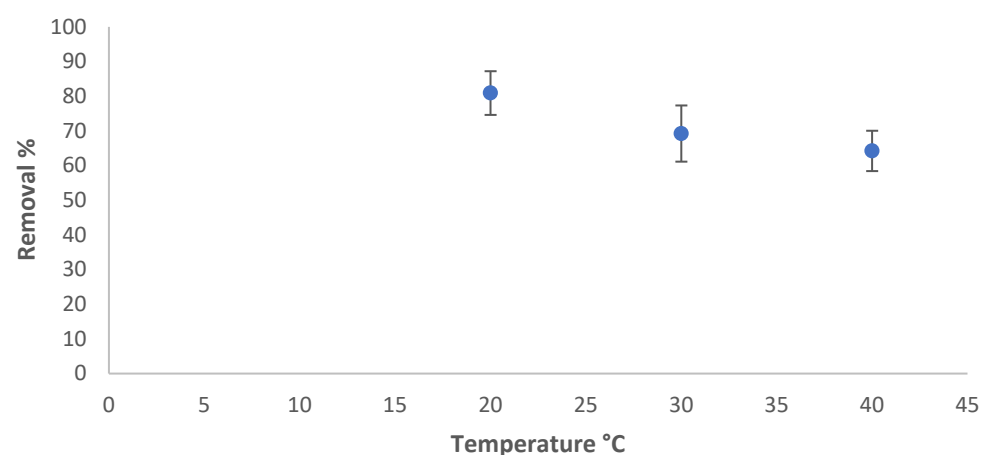

Figure 6. Temperature influence on the removal efficiency %.

3.5.4. Regeneration and Reuse Study

The ability to regenerate for multiple uses without making changes in chemical or physical properties or suffering the loss of adsorption capacity was investigated. The regeneration and reuse tendencies of silica nanoparticles are essential for evaluating their efficiency as excellent sorbents (Figure 7). We performed five runs, and the data show that more than 50% of the azoxystrobin could be removed from the solution in the fifth run.

Although the silica nanoparticles exhibited high adsorption capacity in the first runs, the reusability of the silica nanoparticle sorbent could prolong the control over the adsorption of azoxystrobin from aqueous solutions even after five cycles. This indicates that silica nanoparticles have good reusability and considerable adsorption efficiency.
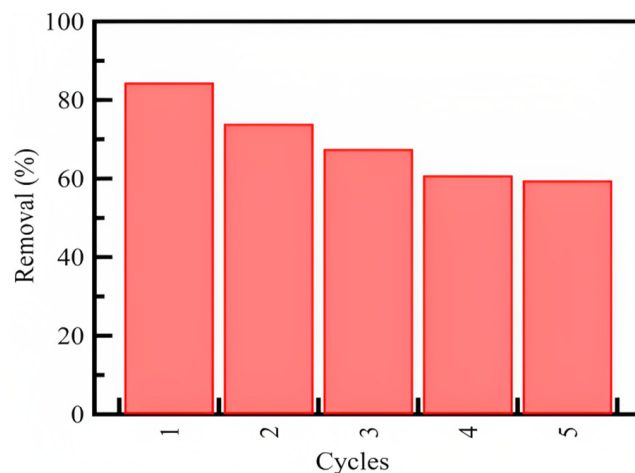
Figure 7. The regeneration and repetitive usage tendency of the SiO_2 nanoparticles on adsorption of azoxystrobin from aqueous solutions.

In general, the results showed that the adsorption efficiency of azoxystrobin was dependent on the adsorbent dosage of silica nanoparticles and the temperature of the solution, and the adsorption capacity increased with decreasing initial azoxystrobin concentration in aqueous solution, indicating the saturation of available active sites on the surface of nanosilica at a higher initial azoxystrobin concentration. These synthesized silica nanoparticles (SiO_2-NPs) were compared with other nanoparticles in terms of the removal efficiency of various pollutants (Table 3).

Table 3. Comparison of the current study with previous studies using different types of nanoparticles to remove pesticides, tetracycline, and naphthalene contamination.

Adsorbent	Pesticide Type	Maximum Adsorption Capacity (mg/g)	References
Phenyl-modified magnetic graphene/ mesoporous silica	Avermectin, Imidacloprid, Pyridaben, Dichlorvos, Acetamiprid, Dursban, Isocarbophos, Phoxim	9.208 (avermectin); 6.404 (imidacloprid); 12.72 (pyridaben); 47.78 (dichlorvos); 5.108 (acetamiprid); 8.010 (dursban); 2.877 (isocarbophos); 8.233 (phoxim)	[42]
Graphene oxide-based silica-coated magnetic nanoparticles functionalized with 2- phenylethylamine	Chloropyriphos, Parathion, Malathion	25.6 (chloropyriphos); 135 (parathion); 61.9 (malathion)	[43]
Surfactant-coated silica nanoparticles	Naphthalene	11.45 (naphthalene)	[44]
Functionalized magnetic nanoparticles	Tetracycline	39.1 to 666.7	[45]
Functionalized multi-walled carbon nanotube	Malathion	5.45–17.11	[46]
The nanocomposite of graphene oxide (GO) and iron oxide (Fe_3O_4) magnetic nanoparticles (MNPs)	Endrin Dieldrin	99 (endrin); 1 (dieldrin)	[47]
Metal-organic framework on graphene oxide	Glyphosate	482.69	[48]
SiO_2-NPs	Azoxystrobin	0.85	This study

3.6. Isothermal and Kinetic Studies of Adsorption Processes

The adsorption equilibrium results were analyzed by calculating the equilibrium concentration of the adsorbate in a liquid phase using the adsorption isotherms and the ratio of the mass of the adsorbate (azoxystrobin) to the weight of the adsorbent (SiO_2-NPs). Using the Langmuir and Freundlich isotherm models, we analyzed the data on the adsorption of azoxystrobin molecules onto the surface of modified SiO_2-NPs. The isothermal data were linearized in Figure 8 using the Langmuir and Freundlich equations. The Langmuir isotherm model was used to determine the KL and Qmax values for the adsorption of azoxystrobin onto SiO_2-NPs (Figure 8A). We calculated the adsorption capacity (Q_{max}) of 0.85 mg/g and a KL of 27,869.8 mg/L. The increased availability of active adsorption sites per volume ratio could be attributed to the increased surface area of SiO_2-NPs and, thus, a more significant percentage of total pore size to volume. The Langmuir model achieved R^2 values as high as 0.9999. R^2 values indicate that the Langmuir model is well suited to describe the adsorption of azoxystrobin onto SiO_2-NPs.
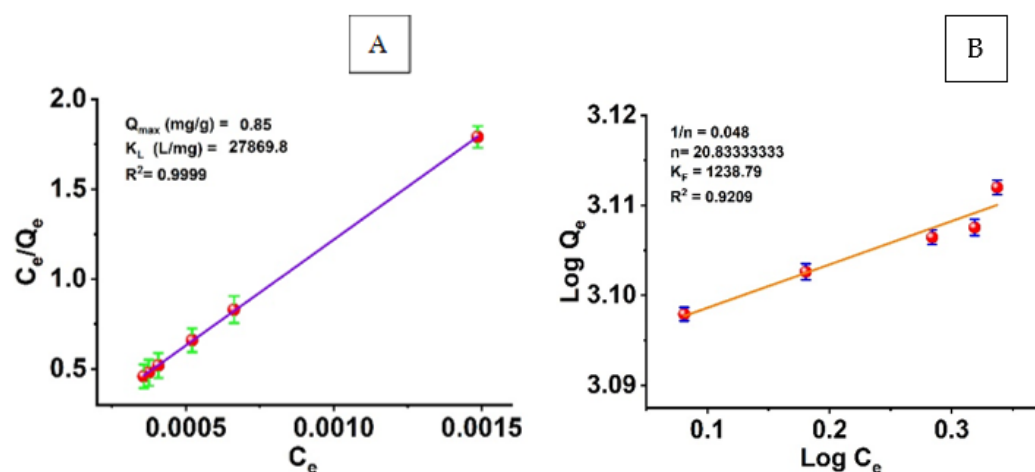

Figure 8. (**A**) Langmuir and (**B**) Freundlich adsorption isotherm models.

The Freundlich model was also used to linearize silica nanoparticles' adsorption isotherms of azoxystrobin removal efficiency (Figure 8B). The Freundlich constants KF and n are plotted in Figure 8B for the experimental data. The correlation coefficient (R^2) was 0.92. For the removal of azoxystrobin from silica nanoparticles, the adsorption isotherms were found to agree well with the Langmuir isotherm model, and the Langmuir adsorption model provided a more accurate representation of the adsorption process than the Freundlich model.

Pseudo-first and pseudo-second-order adsorption kinetics models were used to perform kinetic analysis of the experimental data. These kinetic models can estimate the adsorption rates and mechanisms of azoxystrobin molecules on the functionalized SiO_2-NPs surface. The following equation describes the pseudo-first-order model [49]:

$$Log(q_e - q_t) = \log q_e - k_1 t$$

where q_e and q_t are the adsorption rates of azoxystrobin at equilibrium and at time t (min) in milligrams per gram and milligrams per second, respectively, and its pseudo-first-order rate constant is denoted by the symbol k_1 (min^{-1}). The time required for the adsorption of azoxystrobin onto SiO_2-NPs is shown in Figure 9A as a linear function of log ($q_e - q_t$) versus (t). The rate constants (K_1) and theoretical adsorption capacities (q_e) can be derived from the slopes and intercepts, which are 1.419×10^{-4} min^{-1} and 776.24 mg/g, respectively. The linear formula of the pseudo-second-order model [50] is also described.

$$t/q_t = 1/k_2 q_e^2 + t/q_e$$

where k_2 (g mg^{-1} min^{-1}) is the pseudo-second-order rate constant. As shown in Figure 9B, the plots of t/qt versus t give straight lines with slopes and intercepts corresponding to the pseudo-second-order rate constants (k_2) and theoretical adsorption capacities (q_e) theo, respectively; they are 4.87 g mg^{-1} min^{-1} and 0.0246 mg/g. Comparing the values of correlation coefficients (R^2) and the theoretical adsorption capacities (q_e) theo of the pseudo-first and pseudo-second-order models, we find that the R^2 values (0.9992) of the pseudo-second-order model are higher than those of the pseudo-first-order R^2 model (0.6103). Accordingly, the obtained results of adsorption kinetics follow the pseudo-second-order kinetic model.
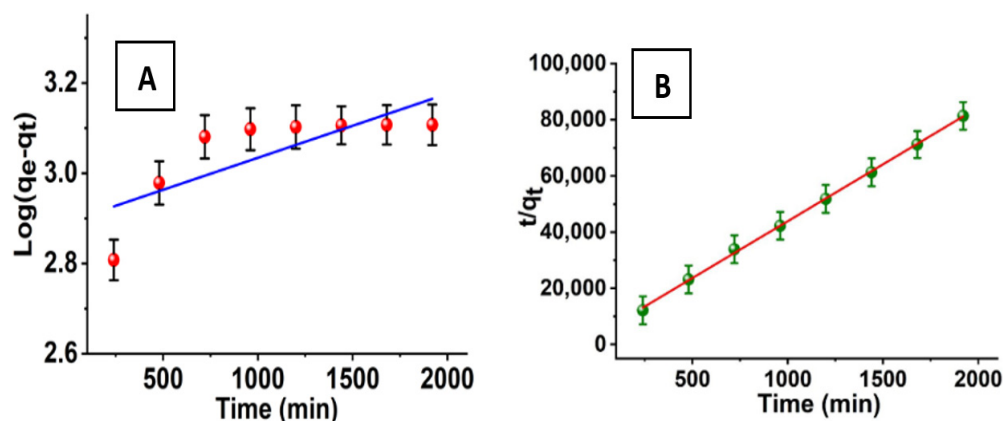

Figure 9. (**A**) Pseudo-first and (**B**) pseudo-second-order kinetic models for the adsorption process.

4. Conclusions

In conclusion, this study is the first to report using SiO$_2$-NPs. They can be used as nano-adsorbents to obtain azoxystrobin from water. SiO$_2$-NPs, with spherical their morphology and high specific surface area, were successfully prepared via the sol–gel method, and the specific surface area of SiO$_2$-NPs was (416.85 m^2/g). Various physicochemical factors, such as azoxystrobin initial concentration, temperature, and adsorbent dose, were investigated during the batch adsorption experiments. The results showed that the percentage removal of azoxystrobin was highly dependent on temperature, and that the removal efficiency of each adsorbent was improved at higher temperature values. The optimum temperature for removing azoxystrobin was 20 °C, while the optimum quantity was 0.05 g. The results showed that the silica adsorbent could be used for five cycles of absorption–desorption of azoxystrobin, indicating that the synthesized nanoparticles had valuable stability and performance. Finally, the results showed that the synthesized nanoparticles could be used as efficient sorbents to remove azoxystrobin from aqueous solutions.

References

1. Wang, W.; Martin, J.C.; Zhang, N.; Ma, C.; Han, A.; Sun, L. Harvesting silica nanoparticles from rice husks. *J. Nano Part Res.* **2011**, *13*, 6981–6990. [CrossRef]
2. Chandrasekhar, S.; Pramada, P.N.; Raghavan, P.; Satyanrayana, K.G. Micro silica from rice husk as a possible substitute for condensed silica fume for high-performance concrete. *J. Mater. Sci. Lett.* **2002**, *21*, 1245–1247. [CrossRef]
3. Mader, H.; Li, X.; Saleh, S.; Link, M.; Kele, P.; Wolfbeis, O.S. Fluorescent silica nanoparticles. *Ann. N. Y. Acad. Sci.* **2008**, *1130*, 218–223. [CrossRef] [PubMed]
4. Ali, R.; Saleh, S.M.; Elshaarawy, R.F. Turn-on pH nano-fluorosensor based on imidazolium salicylaldehyde ionic liquid-labeled silica nanoparticles. *RSC Adv.* **2016**, *6*, 86965–86975. [CrossRef]
5. Saleh, S.M.; Müller, R.; Mader, H.S.; Duerkop, A.; Wolfbeis, O.S. Novel multicolor fluorescently labeled silica nanoparticles for interface fluorescence resonance energy transfer to and from labeled avidin. *Anal. Bioanal. Chem.* **2010**, *398*, 1615–1623. [CrossRef]
6. Saleh, S.M.; Alminderej, F.M.; Ali, R.; Abdallah, O.I. Optical sensor film for metribuzin pesticide detection. *Spectrochim. Acta A Mol. Biomol. Spectrosc.* **2020**, *229*, 117971. [CrossRef]
7. Zhang, W.; Ma, M.; Zhang, X.A.; Zhang, Z.Y.; Saleh, S.M.; Wang, X.D. Fluorescent proteins as efficient tools for evaluating the surface PEGylation of silica nanoparticles. *Methods Appl. Fluoresc.* **2017**, *5*, 024003. [CrossRef]
8. Mellaerts, R.; Houthoofd, K.; Elen, K.; Chen, H.; Van Speybroeck, M.; Van Humbeeck, J.; Augustijns, P.; Mullens, J.; Van den Mooter, G.; Martens, J.A. Aging behavior of pharmaceutical formulations of itraconazole on SBA-15 ordered mesoporous silica carrier material. *Microporous Mesoporous Mater.* **2010**, *130*, 154–161. [CrossRef]
9. Hou, P.; Kawashima, S.; Kong, D.; Corr, D.J.; Qian, J.; Shah, S.P. Modification effects of colloidal nanoSiO$_2$ on cement hydration and its gel property. *Compos. Part B Eng.* **2016**, *45*, 440–448. [CrossRef]
10. Youssif, M.I.; El-Maghraby, R.M.; Saleh, S.M.; Elgibaly, A.A. Sol–Gel Tailored Synthesized Nanosilica for Enhanced Oil Recovery in Water-Wet and Oil-Wet Benthemier Sandstone. *Energy Fuel.* **2018**, *32*, 12373–12382. [CrossRef]
11. Saleh, S.; Younis, A.; Ali, R.; Elkady, E. Phenol removal from aqueous solution using amino-modified silica nanoparticles. *Korean J. Chem. Eng.* **2019**, *36*, 529–539. [CrossRef]
12. Pajonk, G.M. Some applications of silica aerogels. *Colloid Polym. Sci.* **2003**, *281*, 637–651. [CrossRef]
13. Chuiko, A.A. *Medical Chemistry and Clinical Application of Silicon Dioxide*; Nukova Dumka: Kiev, Ukraine, 2003.
14. Saleh, S.M.; Ali, R.; Wolfbeis, O.S. New silica, and polystyrene nanoparticles labeled with longwave absorbing and fluorescent chameleon dyes. *Microchim. Acta* **2011**, *174*, 429–434. [CrossRef]
15. Youssif, M.I.; El-Maghraby, R.M.; Saleh, S.M.; Elgibaly, A. Silica nanofluid flooding for enhanced oil recovery in sandstone rocks. *Egypt. J. Pet.* **2018**, *27*, 105–110. [CrossRef]
16. Kumar, M.N.V.; Sameti, M.; Mohapatra, S.S.; Kong, X.; Lockey, R.F.; Bakowsky, U.; Lindenblatt, G.; Schmidt, C.H.; Lehr, C.-M. Cationic silica nanoparticles as gene carriers: Synthesis, characterization and transfection efficiency in vitro and in vivo. *J. Nano Sci. Nano Technol.* **2004**, *4*, 876–881. [CrossRef] [PubMed]
17. Younis, A.M.; Elkady, E.M.; Saleh, S.M. Novel eco-friendly amino-modified nanoparticles for phenol removal from aqueous solution. *Environ. Sci. Pollut. Res.* **2020**, *27*, 30694–30705. [CrossRef]
18. Moghimi, S.M.; Hunter, A.C.; Murray, J.C. Nanomedicine: Current status and prospects. *FASEB J.* **2005**, *19*, 311–330. [CrossRef]
19. Slowing, I.I.; Trewyn, B.G.; Giri, S.; Lin, V.S.Y. Mesoporous silica nanoparticles for drug delivery and biosensing applications. *Adv. Funct. Mater.* **2007**, *17*, 1225–1236. [CrossRef]
20. Slowing, I.I.; Vivero-Escoto, J.L.; Wu, C.W.; Lin, V.S. Mesoporous silica nanoparticles as controlled release drug delivery and gene transfection carriers. *Adv. Drug Deliv. Rev.* **2008**, *60*, 1278–1288. [CrossRef]
21. Gurav, J.L.; Jung, I.K.; Park, H.H.; Kang, E.S.; Nadargi, D.Y. Silica aerogel: Synthesis and applications. *J. Nanomater.* **2010**, *2010*, 409310. [CrossRef]
22. Napierska, D.; Thomassen, L.C.; Lison, D.; Martens, J.A.; Hoet, P.H. The nano-silica hazard: Another variable entity. *Part. Fibre Toxicol.* **2010**, *7*, 39. [CrossRef] [PubMed]
23. Shin, Y.; Lee, D.; Lee, K.; Ahn, K.H.; Kim, B. Surface properties of silica nanoparticles modified with polymers for polymer nanocomposite applications. *J. Ind. Eng. Chem.* **2008**, *14*, 515–519. [CrossRef]
24. Zou, H.; Wu, S.; Shen, J. Polymer/silica nanocomposites: Preparation, characterization, properties, and applications. *Chem. Rev.* **2008**, *108*, 3893–3957. [CrossRef]
25. Subbiah, R.; Veerapandian, M.; Yun, K.S. Nanoparticles: Functionalization and multifunctional applications in biomedical sciences. *Curr. Med. Chem.* **2010**, *17*, 4559–4577. [CrossRef] [PubMed]
26. Bhagiyalakshmi, M.; Yun, L.J.; Anuradha, R.; Jang, H.T. Utilization of rice husk ash as silica source for the synthesis of mesoporous silicas and their application to CO$_2$ adsorption through TREN/TEPA grafting. *J. Hazard Mater.* **2010**, *175*, 928–938. [CrossRef]
27. Rahman, I.A.; Padavettan, V. Synthesis of silica nanoparticles by Sol-gel: Size-dependent Properties, Surface Modification and Applications in Silica-Polymer Nanocomposites—A Review. *J. Nanomater.* **2012**, *2012*, 132424. [CrossRef]
28. Bernardos, A.; Kourimska, L. Applications of Mesoporous Silica Materials in Food—A Review. *Czech J. Food Sci.* **2013**, *31*, 99–107. [CrossRef]
29. Hassan, A.F.; Abdelghny, A.M.; Elhadidy, H.; Youssef, A.M. Synthesis and characterization of high surface area nano silica from rice husk ash by surfactant-free sol-gel method. *J. Sol-Gel Sci. Technol.* **2014**, *69*, 465–472. [CrossRef]

30. Brinker, C.J.; Scherer, G.W. *Sol-Gel Science: The Physics and Chemistry of Sol-Gel Processing*; Academic Press Inc.: San Diego, CA, USA, 1990; p. 907.

31. Amirhandeh, S.Z.H.; Salem, A.; Salem, S. Treatment of tannery wastewater by silica nanoparticles produced from rice husk ash via a green route. *Environ. Sci. Pollut. Res. Int.* **2023**, *30*, 13039–13047. [CrossRef]

32. Gehrke, I.; Geiser, A.; Somborn-Schulz, A. Innovations in nanotechnology for water treatment. *Nanotechnol. Sci. Appl.* **2015**, *8*, 1–17. [CrossRef]

33. Sharma, P.; Prakash, J.; Kaushal, R. An insight into the green synthesis of SiO_2 nanostructures as a novel adsorbent for removal of toxic water pollutants. *Environ. Res.* **2022**, *212*, 113328. [CrossRef] [PubMed]

34. Ui, S.W.; Lim, S.J.; Lee, S.H.; Choi, S.C. Control of the size and morphology of nano-size silica particles using a sodium silicate solution. *J. Ceram. Process. Res.* **2009**, *10*, 553–558.

35. Mushtaq, N.; Singh, D.V.; Bhat, R.A.; Dervash, M.A.; Hameed, O.B. Freshwater contamination: Sources and hazards to aquatic biota. *Freshw. Pollut. Dyn. Remediat.* **2020**, 27–50. [CrossRef]

36. Manasa, R.L.; Mehta, A. Wastewater: Sources of pollutants and its remediation. *Environ. Biotechnol.* **2020**, *2*, 197–219.

37. Vela, N.; Fenoll, J.; Garrido, I.; Pérez-Lucas, G.; Flores, P.; Hellín, P.; Navarro, S. Reclamation of agro-wastewater polluted with pesticide residues using sunlight activated persulfate for agricultural reuse. *Sci. Total Environ.* **2019**, *660*, 923–930. [CrossRef]

38. Sutherland, D.L.; Ralph, P.J. Microalgal bioremediation of emerging contaminants-opportunities and challenges. *Water Res.* **2019**, *164*, 114921. [CrossRef]

39. Nguyen, X.H.; Tran, N.A.; Nguyen, T.T.H.; Dao, T.T.N. Nanosilica synthesis and application for lead treatment in water. *J. Vietnam. Environ.* **2018**, *9*, 255–263. [CrossRef]

40. Srivastava, A.; Kumari, M.; Ramanathan, A.; Selvaraj, K.; Prasad, B.; Prasad, K.S. Removal of fluoride from aqueous solution by mesoporous silica nanoparticles functionalized with chitosan derived from mushroom. *J. Macromol. Sci. Part A* **2020**, *9*, 619–627. [CrossRef]

41. Yao, J.; Cui, B.; Zhao, X.; Zhi, H.; Zeng, Z.; Wang, Y.; Sun, C.; Liu, G.; Gao, J.; Cui, H. Antagonistic effect of azoxystrobin poly (lactic acid) microspheres with controllable particle size on *Colletotrichum higginsianum* Sacc. *Nanomaterials* **2018**, *8*, 857. [CrossRef]

42. Wang, X.; Wang, H.; Lu, M.; Teng, R.; Du, X. Facile synthesis of phenyl-modified magnetic graphene/mesoporous silica with hierarchical bridge-pore structure for efficient adsorption of pesticides. *Mater. Chem. Phys.* **2017**, *198*, 393–400. [CrossRef]

43. Wanjeri, V.W.O.; Sheppard, C.J.; Prinsloo, A.R.E.; Ngila, J.C.; Ndungu, P.G. Isotherm and kinetic investigations on the adsorption of organophosphorus pesticides on graphene oxide based silica-coated magnetic nanoparticles functionalized with 2-phenylethylamine. *J. Environ. Chem. Eng.* **2018**, *6*, 1333–1346. [CrossRef]

44. Chaudhary, S.; Sharma, P.; Kaur, A.; Kumar, R.; Mehta, S.K. Surfactant coated silica nanoparticles as smart scavengers for adsorptive removal of naphthalene. *J. Nanosci. Nanotechnol.* **2018**, *18*, 3218–3229. [CrossRef] [PubMed]

45. Wang, T.; Ai, S.; Zhou, Y.; Luo, Z.; Dai, C.; Yang, Y.; Luo, L. Adsorption of agricultural wastewater contaminated with antibiotics, pesticides, and toxic metals by functionalized magnetic nanoparticles. *J. Environ. Chem. Eng.* **2018**, *6*, 6468–6478. [CrossRef]

46. Massad, Y.; Hanbali, G.; Jodeh, S.; Hamed, O.; Bzour, M.; Dagdag, O.; Samhan, S. The efficiency of removal of organophosphorus malathion pesticide using functionalized multi-walled carbon nanotube: Impact of Dissolved Organic Matter (DOM). *Sep. Sci. Technol.* **2022**, *57*, 1–12. [CrossRef]

47. Shrivas, K.; Ghosale, A.; Nirmalkar, N.; Srivastava, A.; Singh, S.K.; Shinde, S.S. Removal of endrin and dieldrin isomeric pesticides through stereoselective adsorption behavior on the graphene oxide-magnetic nanoparticles. *Environ. Sci. Pollut. Res.* **2017**, *24*, 24980–24988. [CrossRef]

48. Yang, Q.; Wang, J.; Zhang, W.; Liu, F.; Yue, X.; Liu, Y.; Wang, J. Interface engineering of metal-organic framework on graphene oxide with enhanced adsorption capacity for organophosphorus pesticide. *Chem. Eng. J.* **2017**, *313*, 19–26. [CrossRef]

49. Hameed, B.H.; Rahman, A.A. Removal of phenol from aqueous solutions by adsorption onto activated carbon prepared from biomass material. *J. Hazard. Mater.* **2008**, *160*, 576–581. [CrossRef]

50. Yuh-Shan, H. Citation review of Lagergren kinetic rate equation on adsorption reactions. *Scientometrics* **2004**, *59*, 171–177. [CrossRef]